Unbalanced Model and Power-Flow Analysis of Microgrids and Active Distribution Systems

Mohamed Zakaria Kamh, *Graduate Student Member, IEEE*, and Reza Iravani, *Fellow, IEEE*

***Abstract*—This paper presents a three-phase power-flow algorithm, in the sequence-component frame, for the microgrid (μgrid) and active distribution system (ADS) applications. The developed algorithm accommodates single-phase laterals, unbalanced loads and lines, and three/four-wire distribution lines. This paper also presents steady-state sequence-component frame models of distributed energy resource (DER) units for the developed power-flow approach under balanced/unbalanced conditions. The DER models represent the synchronous-generator based and the electronically-coupled DER units. Both constant power (PQ) and regulated-voltage (PV) modes of operation of DER units are considered. The application of the developed power-flow method for two study systems is presented. The study results are validated based on comparison with the detailed solution of the system differential equations in time domain, using the PSCAD/EMTDC software tool.**

***Index Terms*—Active distribution systems, distributed energy resources (DER), microgrids, single-phase laterals, three-phase power flow.**

I. Introduction

DRIVEN by environmental, economical, and technical incentives, the integration of distributed energy resources (DER) units into distribution networks close to the loads, is emerging as a complementary infrastructure to the traditional central power plants [1]. A DER unit is either a distributed generation (DG) unit, a distributed storage (DS) unit, or a hybrid of the two [2]. Proliferation of DER units, primarily at the distribution voltage levels, has also brought about concepts of the microgrid (μgrid) [3]–[5] and the active distribution system (ADS) [6]–[8]. The μgrid concept is well defined in the technical literature. An ADS is a distribution network with arbitrary power flow along the network feeders, where variables are measured (or estimated) and controlled by means of various devices (e.g., DER units, on-load tap changers, and transformer), based on a centralized and intelligent system. The central control system is capable of making decisions and operating the system based on monitoring the network conditions [7]. The ADS ultimate goal is to allow safe penetration of DER units into the current distribution networks and maintain the system stable and reliable [8].

Manuscript received July 13, 2009; revised November 13, 2009. First published April 05, 2010; current version published September 22, 2010. Paper no. TPWRD-00522-2009.

The authors are with the Department of Electrical and Computer Engineering, University of Toronto, Toronto, ON M5S 3G4, Canada (e-mail: mohamed.kamh@ieee.org; iravani@ecf.utoronto.ca).

Color versions of one or more of the figures in this paper are available online at http://ieeexplore.ieee.org.

Digital Object Identifier 10.1109/TPWRD.2010.2042825

The first requirement for planning, operation, control, protection, and management of the μgrid (and ADS) is the availability of accurate power-flow analysis results. The conventional power-flow analysis methods, based on the system positive-sequence representation, that are widely used for large power transmission systems, are not directly applicable to the μgrids and ADS [9]. The reasons are the:

- relatively high degree of imbalance due to the inherent untransposed structure of three-wire and/or four-wire three-phase power distribution lines, presence of single-phase laterals, single and two-phase loads, unbalanced three-phase loads [10],
- presence of three-phase and single-phase electronically-coupled DG and DS units with various control strategies and operational modes [11], [12],
- presence of different types of three-phase rotating machine-based DG units with various control strategies [13],
- presence of non-dispatchable DG units, for example, wind and photovoltaic units [14].

Moreover, the production-grade power-flow software tools, which originally have been developed for large-system, are not tailored for the μgrid and ADS analysis. The reason is that they lack the flexibility to accommodate DER models and operating characteristics, particularly those of electronically-coupled DER units [15]. Another limitation is that the existing technical literature on the steady-state modeling of electronically-coupled DER units assumes only positive-sequence DER representation for power-flow analysis [15]–[17].

The concept of three-phase power-flow analysis has been extensively addressed in the literature [10], [18]–[27], and the applicable methods are classified according to the network structure and the adopted reference frame. Based on the phase-frame approach [10], [22]–[24], (i) the forward-backward sweep method [18], and (ii) the compensation method [19]–[21] have been proposed for power-flow analysis of radial feeders and weakly meshed grids, respectively. The power-flow analysis of the loop (ring) network structure or the general network structures are conducted based on Newton-Raphson [24]–[26] and Gauss and/or Gauss-Seidel [10], [22], [23] methods. The sequence-components frame has been used in [25]–[27] to develop a three-phase power-flow solver for general network topologies with synchronous generating units. Using the sequence-components frame in the power-flow analysis effectively reduces the problem size and the computational burden as compared to the phase-frame approach. Moreover, due to the weak coupling between the three sequence networks, the system equations can be solved using parallel programming [26].

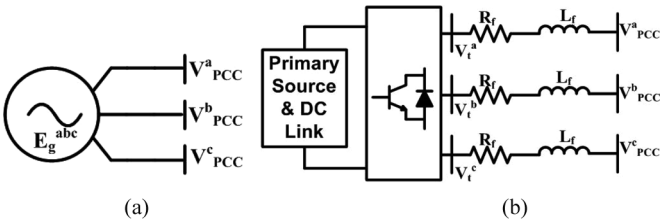

Fig. 1. Schematic diagram of DER unit: (a) SG unit. (b) Electronically-coupled unit.

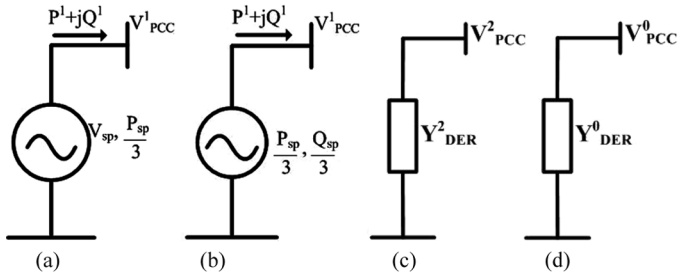

Fig. 2. Generalized sequence-component frame model of DER unit for power-flow analysis.

Motivated by the aforementioned merits of the sequence components for power-flow analysis, this paper develops a sequence-frame power-flow solver for the μgrid and the ADS. The developed power-flow solver modifies the algorithms presented in [25] and [26] to incorporate models of electronically-coupled DER units that include their control characteristics under balanced/unbalanced grid conditions. In addition, this paper exploits the concept of the coincidence factor [28], [29] to accommodate single-phase laterals in the developed sequence-frame power-flow solver. The power-flow algorithm also accommodates (i) three-phase distribution transformers, (ii) three-phase three- and four-wire distribution lines, and (iii) three-phase (ub)balanced constant power and constant impedance loads. The accuracy and validity of the developed power-flow algorithm, including the DER and the single-phase lateral models, were tested on two study-systems and the results of several case-studies are compared with those obtained from the time-domain analysis in the PSCAD/EMTDC environment.

II. Steady-State DER Models

This section presents generalized sequence-component frame models of the:

- three-phase, directly-interfaced, synchronous generator (SG)-based DG unit,
- three-phase electronically-coupled DER unit interfaced via a three-phase, three-wire VSC. It is assumed that the VSC controllers tightly regulate the DC-link voltage, and thus the primary source does not affect the steady-state model of the unit with respect to its point of connection to the host μgrid (or ADS). This, in turn, implies that in case of intermittent DG units (e.g., wind and photovoltaic units), adequate storage is interfaced to the VSC dc-side to enable its operation as dispatchable DG units.

The models are incorporated in the developed power-flow algorithm of Section III. Fig. 1 shows a schematic diagram of a DER unit connected to the host μgrid (or ADS) at the point of common coupling (PCC). It should be noted that the developed DER model can be enhanced to represent other types of three-phase VSC-coupled DER units (e.g., the four-wire VSC-coupled DER units), the permanent-magnet synchronous generator driven by a micro-turbine or a wind turbine, and the doubly-fed asynchronous generator.

The developed model accommodates both PQ and PV modes of operation for directly-coupled and electronically-coupled DER units. Under both operating modes, the positive sequence voltage of the PCC is used for synchronization [12]. It should be noted that the PCC voltage might be contaminated with the negative and zero sequence voltage components due to the asymmetries and imperfections in the system. This indicates that if the DER unit is synchronized with and controlled to generate only positive sequence components, its current exchange with the μgrid (or the ADS) can include negative and zero sequence components depending on the control strategy. The VSC-coupled DER units can be augmented with additional controllers to mitigate the negative-sequence current and only exchange positive-sequence current with the μgrid [11]. In such a case, the terminal voltage of the VSC-coupled DER unit includes both positive and negative sequence voltage components. Thus, for both the SG and the VSC-coupled DER units, the active power output of the DER unit is determined based on the positive sequence voltages and currents. The same concept is also adopted for the reactive power controller when the PQ operating mode is implemented.

A. Positive Sequence Model

Based on the above discussion, Fig. 2 represents the proposed generalized sequence-component frame model of both the three-phase directly interfaced SG unit and the three-phase VSC-coupled DER unit. The positive-sequence model of a DER unit also represents its control strategy. If the unit operates in the PV mode (Fig. 2(a)), it is modeled as an ideal voltage source behind the PCC bus. Under this mode of operation, the magnitude of the positive-sequence component of the DER terminal voltage ($|V^1_{PCC}|$) and the corresponding injected positive-sequence real power (P^1), both in per-unit, are given by

$$\left|V^1_{PCC}\right| = V_{sp} \tag{1}$$

$$P^1 = P_{total-injected}/3 \tag{2}$$

where V_{sp} and $P_{total-injected}$ are the per-unit positive-sequence terminal voltage and the total three-phase injected active power of the DER unit, respectively.

If the DER unit operates in the PQ mode, its positive-sequence representation is a constant power source (or negative constant power load) as shown in Fig. 2(b), [30]. Thus, the positive-sequence reactive power (Q^1) injected by the DER unit, in per-unit, is

$$Q^1 = Q_{total-injected}/3 \tag{3}$$

where $Q_{total-injected}$ is the total three-phase reactive power injected by the DER unit. The factor 1/3 in (2) and (3) is used to calculate the sequence-frame power components from their

phase-frame counterparts, assuming the same base-power is used in both reference frames. Since the power and voltages to be regulated are often (practically) those of the PCC bus, the positive sequence impedance of the unit and its terminal voltage are not shown in Fig. 2(a) and Fig. 2(b).

B. Negative and Zero Sequence Models

Depending on the type (SG or VSC-coupled DER) and the control strategy [11] of the DER unit, the negative and zero sequence current components can also be exchanged between the μgrid (ADS) and the DER unit. The proposed generalized negative and zero sequence models of the SG and the three-wire VSC-coupled DER units of Fig. 1 are shown in Fig. 2(c) and (d), respectively.

1) SG Unit: For the SG unit, the zero and negative sequence admittances ($Y_{DER}^{0,2}$) of the generalized model are [31], [32]

$$Y_{DER}^{0,2} = 1/\left(R_{SG}^{0,2} + \jmath X_{SG}^{0,2}\right) \tag{4}$$

where

$$\begin{aligned} R_{SG}^{2} &= R_{a-SG} \\ R_{SG}^{0} &= R_{a-SG} + 3R_{n-SG} \end{aligned} \tag{5}$$

and

$$\begin{aligned} X_{SG}^{2} &= \left(X''_{d-unsat} + X''_{q-unsat}\right)/2 \\ X_{SG}^{0} &= \frac{X_{SG}^{2}}{4} + 3X_{n-SG} \end{aligned} \tag{6}$$

where $X''_{d-unsat}(X''_{q-unsat})$ is the direct (quadrature) unsaturated sub-transient reactance, $X_{n-SG}(R_{n-SG})$ is the reactance (resistance) between the neutral of the SG and the ground, and R_{a-SG} is the armature resistance of the SG.

2) Three-Wire VSC-Coupled DER Unit: The magnitude of the negative sequence admittance for a three-wire VSC-coupled DER unit is determined based on the control strategy of the unit. If the unit is controlled only to generate positive-sequence voltage [12], then the negative sequence admittance of the DER model, Y_{DER}^{2}, is

$$Y_{DER}^{2} = 1/Z_f \tag{7}$$

where Z_f is the equivalent series impedance of the VSC output filter between the PCC and the short-circuited VSC terminals. The VSC output filter is used to reduce the harmonic current injected in the utility system [33]. The simplest output filter topology is a first order series-connected inductor Fig. 1(b), for which Z_f is given by

$$Z_f = R_f + \jmath X_f \tag{8}$$

where $X_f(R_f)$ is the VSC output filter net reactance (resistance). Other output filter configurations are reported in [34]. These alternative configurations lie under either one of the two topologies shown in Fig. 3. The equivalent series impedance,

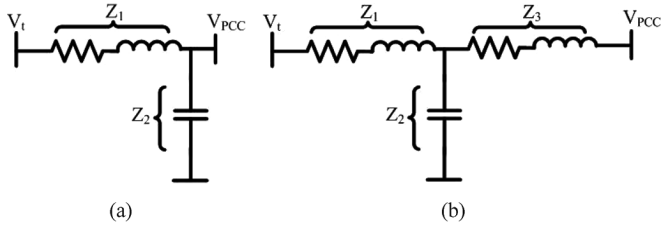

Fig. 3. Alternative VSC output filter configurations.

Z_f, for the filter configurations shown in Fig. 3(a) and Fig. 3(b), is calculated as

$$Z_f = \frac{Z_1 Z_2}{Z_1 + Z_2} \tag{9}$$

$$Z_f = Z_3 + \frac{Z_1 Z_2}{Z_1 + Z_2} \tag{10}$$

where Z_1, Z_2, and Z_3 are shown in Fig. 3.

However, if the unit is controlled to inject balanced three-phase current components [11], that is, operation based on dq-current control strategy, then the negative sequence admittance of the model is

$$Y_{DER}^{2} = 0. \tag{11}$$

In both cases, the zero sequence admittance of the three-wire VSC-coupled DER unit is

$$Y_{DER}^{0} = 0. \tag{12}$$

The negative and zero sequence admittance of each DER unit is substituted in the corresponding bus admittance matrix.

III. Three-Phase Power-Flow Algorithm

This section presents an algorithm to handle DER units and single-phase laterals within the sequence-frame power-flow program. Fig. 4 shows the flow chart of the developed power-flow program including the proposed models of DER units and single-phase laterals.

The first step of the proposed approach is to decompose the μgrid (ADS) into a three-phase section and single-phase laterals. Then each single-phase lateral and its associated loads are lumped and represented by a single-phase load at the node where the lateral is connected to the three-phase system, using the concept of coincidence factor (CF) [28], [29]. Hereafter, this node is referred to as the "head node." The equivalent "lumped" load of the lateral is [35]

$$S_{equiv} = CF \times \sum_{k=1}^{N_{loads}} S_k \tag{13}$$

where N_{loads} is the number of loads on the lateral, and the coincidence factor (CF) is determined based on N_{loads} as [35]

$$CF = 0.6 \times \left(1 + \frac{1}{N_{loads}}\right). \tag{14}$$

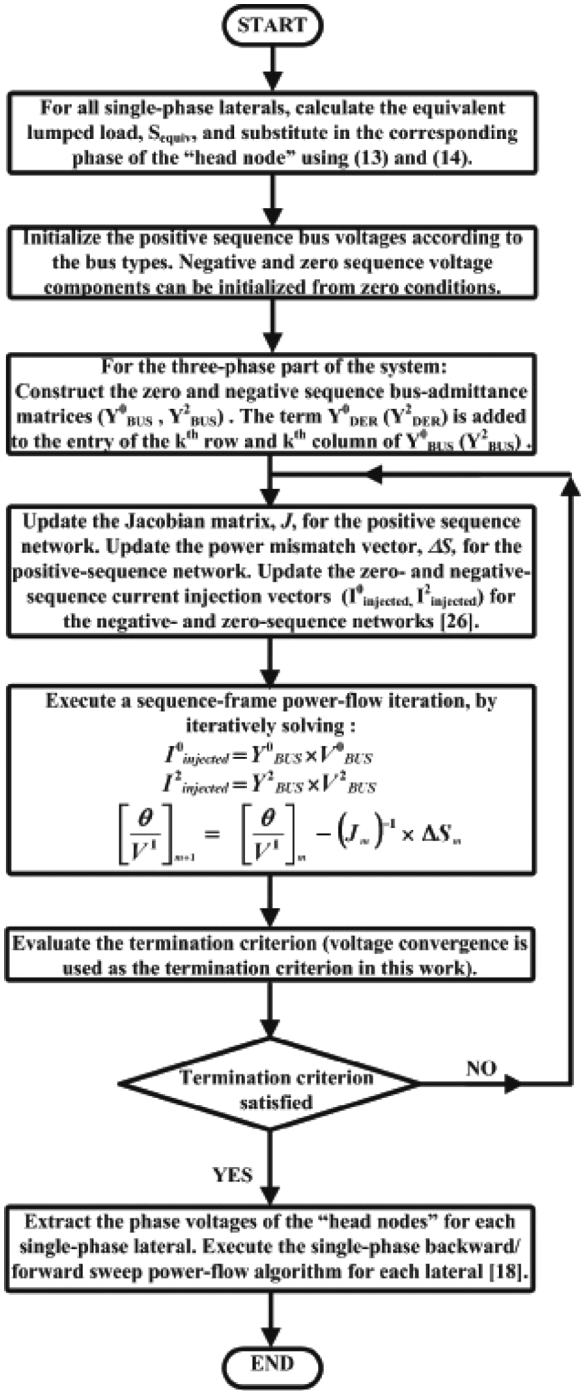

Fig. 4. Flowchart of the developed three-phase power-flow algorithm.

It should be noted that the coincidence factor method is not recommended if the single-phase lateral is equipped with voltage regulating devices or single-phase voltage-controlled DER units. However, to the best of our knowledge, the existing single-phase laterals (in North America) have neither of these two features.

In Fig. 4, $I^0_{injected}(I^2_{injected})$ is the $n \times 1$ zero- (negative) sequence injected current vector, where n is the number of the system buses. The kth entry of $I^0_{injected}(I^2_{injected})$ is formulated by adding the corresponding injected zero- (negative-) sequence components of the loads and the compensation currents of the untransposed distribution power lines connected to the kth bus [26]. Detailed modeling and the model integration of the three-phase untransposed power lines, three-phase transformers, and three-phase (un)balanced loads in a sequence-frame power-flow solver are available in [25] and [26].

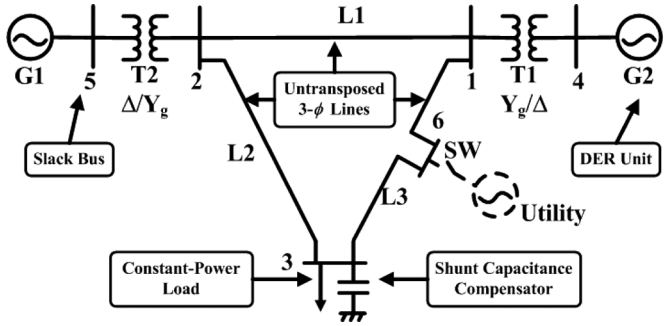

Fig. 5. Single line diagram of System-I.

Unlike the approach of [27] that requires executing the backward-forward sweep subroutine subsequent to each sequence-frame power-flow iteration in a coupled fashion, Fig. 4 indicates that the proposed approach fully decouples the two subroutines by executing the backward/forward sweep algorithm only once after the final convergence of the sequence-frame power-flow algorithm. Thus, the decoupled algorithm of Fig. 4 is expected to substantially reduce the execution time and the computational burden as compared to the coupled approach. This is shown in Section IV.

IV. Case Studies and Validations

To demonstrate the application of the developed power-flow method and validate the accuracy of the results, the power-flow algorithm of Fig. 4 was implemented in MATLAB environment and used to investigate two study systems with different sizes and topologies. The power system sparsity is exploited by using the existing MATLAB functions dedicated to solve large and sparse systems of simultaneous linear equations.

A. System-I

A single line diagram of System-I, which includes six buses, is shown in Fig. 5. The system of Fig. 5 is selected since it is adequately small to be modeled in detail in a time-domain simulation tool, and thus the results can be used for verification of the developed DER models and the sequence-frame power-flow part of the algorithm of Fig. 4. System-I represents an autonomous (islanded) μgrid when switch SW is open and the system can be effectively reduced to a five-bus system. This scenario is considered in this work. The system includes untransposed lines, unbalanced loads, and distribution transformers. The system also includes a three-phase shunt capacitance compensator which is modeled as a three-phase constant impedance [25]. To present a more realistic scenario for the μgrid applications, the base power is selected at 1 MVA instead of 33.33 MVA as specified in [25]. The original system parameters are given in [25].

To validate the power-flow results obtained from the algorithm of Fig. 4 and the developed DER models of Fig. 2, a detailed time-domain model of System-I, in the PSCAD/EMTDC

TABLE I
RESULTS OF CASE 1 OF SYSTEM-I. A:PSCAD/EMTDC RESULTS, B: DEVELOPED SOFTWARE RESULTS

Bus	Phase A				Phase B				Phase C			
	Magnitude (p.u.)		Angle (degrees)		Magnitude (p.u.)		Angle (degrees)		Magnitude (p.u.)		Angle (degrees)	
	A	B	A	B	A	B	A	B	A	B	A	B
1	1.01	1.01	33.12	33.11	1.04	1.03	-86.473	-86.469	1.02	1.03	152.53	152.5
2	1.01	1.02	28.88	28.87	1.03	1.03	-90.93	-90.926	1.02	1.02	148.21	148.25
3	0.99	0.99	24.58	24.58	1.02	1.02	-95.0	-95.0	0.98	0.97	144.9	144.94
4	1.05	1.05	8.48	8.48	1.049	1.049	-111.4	-111.36	1.05	1.05	128.41	128.41
5	1.05	1.05	0.02	0.02	1.04	1.04	-119.3	-119.89	1.05	1.05	119.83	119.88

TABLE II
RESULTS OF CASE 2 OF SYSTEM-I. A: PSCAD/EMTDC RESULTS, B: DEVELOPED SOFTWARE RESULTS

Bus	Phase A				Phase B				Phase C			
	Magnitude (p.u.)		Angle (degrees)		Magnitude (p.u.)		Angle (degrees)		Magnitude (p.u.)		Angle (degrees)	
	A	B	A	B	A	B	A	B	A	B	A	B
1	0.99	1.0	33.472	33.478	1.05	1.05	-85.85	-85.85	1.03	1.02	151.72	151.75
2	1.0	1.0	28.98	28.98	1.04	1.04	-90.61	-90.61	1.02	1.01	147.86	147.87
3	0.97	0.98	24.47	24.47	1.03	1.03	-94.41	-94.41	0.98	0.98	144.52	144.52
4	1.03	1.03	7.91	7.92	1.05	1.05	-110.25	-110.26	1.07	1.06	128.04	128.04
5	1.05	1.04	-0.052	-0.052	1.04	1.04	-119.78	-119.8	1.05	1.05	119.86	119.86

TABLE III
RESULTS OF CASE 3 OF SYSTEM-I. A: PSCAD/EMTDC RESULTS, B: DEVELOPED SOFTWARE RESULTS

Bus	Phase A				Phase B				Phase C			
	Magnitude (p.u.)		Angle (degrees)		Magnitude (p.u.)		Angle (degrees)		Magnitude (p.u.)		Angle (degrees)	
	A	B	A	B	A	B	A	B	A	B	A	B
1	1.05	1.05	15.93	15.93	1.06	1.07	-104.5	-104.4	1.05	1.05	135.1	135.1
2	1.05	1.05	17.39	17.38	1.06	1.06	-103.33	-103.3	1.04	1.05	136.98	137.01
3	1.04	1.04	14.64	14.64	1.07	1.07	-105.23	-105.25	1.04	1.05	133.76	133.75
4	1.04	1.04	-9.36	-9.35	1.05	1.06	-128.93	-128.9	1.05	1.05	110.05	110.07
5	1.04	1.04	-0.96	-0.958	1.04	1.03	-121.03	-121	1.04	1.04	118.91	118.91

TABLE IV
RESULTS OF CASE-4 OF SYSTEM-I. A: PSCAD/EMTDC RESULTS, B: DEVELOPED SOFTWARE RESULTS

Bus	Phase A				Phase B				Phase C			
	Magnitude (p.u.)		Angle (degrees)		Magnitude (p.u.)		Angle (degrees)		Magnitude (p.u.)		Angle (degrees)	
	A	B	A	B	A	B	A	B	A	B	A	B
1	1.04	1.04	17.44	17.43	1.05	1.04	-102.78	-102.76	1.03	1.04	136.89	136.8
2	1.05	1.04	18.48	18.482	1.05	1.05	-101.96	-101.95	1.04	1.03	138.22	138.13
3	1.04	1.04	16.02	16.0	1.05	1.06	-103.668	-103.65	1.03	1.04	135.26	135.16
4	1.03	1.03	-6.772	-6.774	1.04	1.043	-126.496	-126.483	1.04	1.03	112.84	112.76
5	1.04	1.05	-0.87	-0.87	1.04	1.05	-120.884	-120.872	1.03	1.04	119.09	119.01

environment, is also developed. G1 is the slack-bus, and is modeled as an ideal voltage source behind an impedance. It should be noted that in order to handle the active and reactive power limits of the slack bus in an islanded μgrid, the distributed slack bus concept is potentially and advantageous alternative, although it has not been exploited in this work. The load at Bus-3 is represented as a constant-power, star-connected load. Corresponding to the following four case studies, G2 represents either of the following DER units:

Case 1) An SG unit equipped with voltage regulator and active power controller (an SG operating in the PV mode).

Case 2) A voltage-controlled three-wire VSC-coupled DER unit equipped with voltage regulator and active power controllers (a three-phase three-wire VSC-coupled DER unit operating in the PV mode).

Case 3) An SG unit with active and reactive power control (an SG in the PQ mode of operation).

Case 4) A current-controlled three-wire VSC-coupled DER unit equipped with the dq-current controllers [12] (a three-phase three-wire VSC-coupled DER unit operating in the PQ mode).

For the first two cases, the voltage controller of the DER unit adjusts the positive sequence voltage component of Bus-4 at 1.05 p.u. For the last two cases, the DER unit is controlled to inject 1 p.u. active power at unity power-factor. The study results are summarized in Tables I–IV.

Tables I and II show that the magnitude of the phase-voltages of Bus-4 is not 1.05 p.u. However, the positive-sequence voltage component is successfully regulated at 1.05 p.u. as required. This validates the PV model representation for both the SG and the three-wire VSC-coupled DER units. Moreover, the positive-sequence components of the bus-voltages, given in Tables III and IV, and the system parameters, given in [25], are used to evaluate the positive-sequence active and reactive power components injected by G2 at Bus-4. The power injected by G2

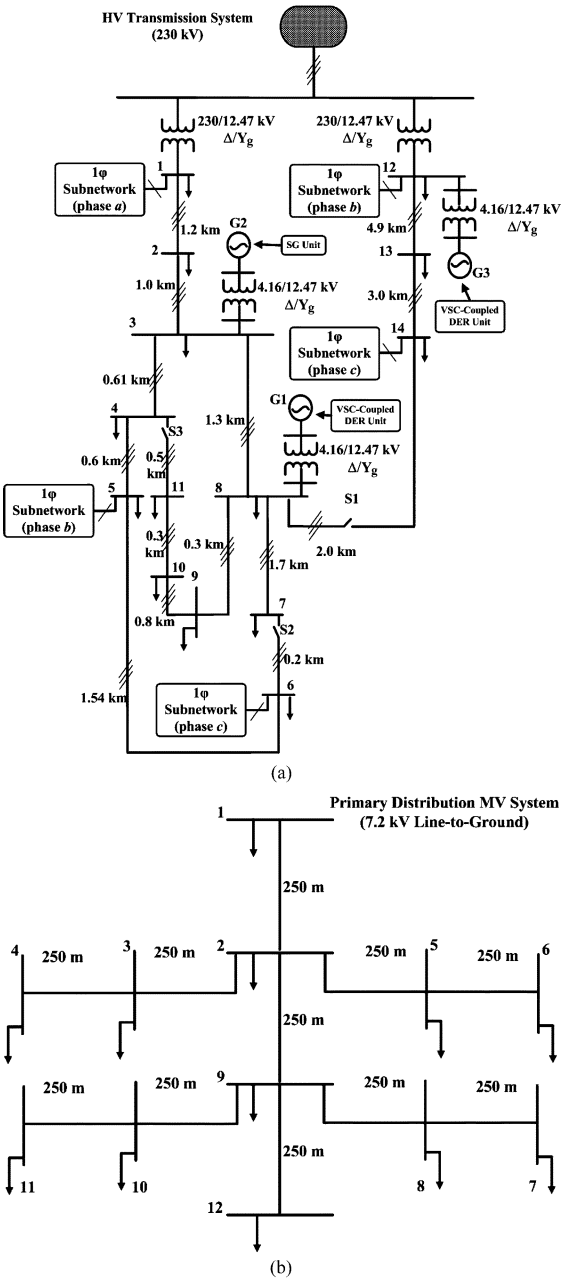

Fig. 6. Single-line diagram of System-II [35]. (a) Three-phase part of System-II. (b) Single-phase subnetwork of System-II.

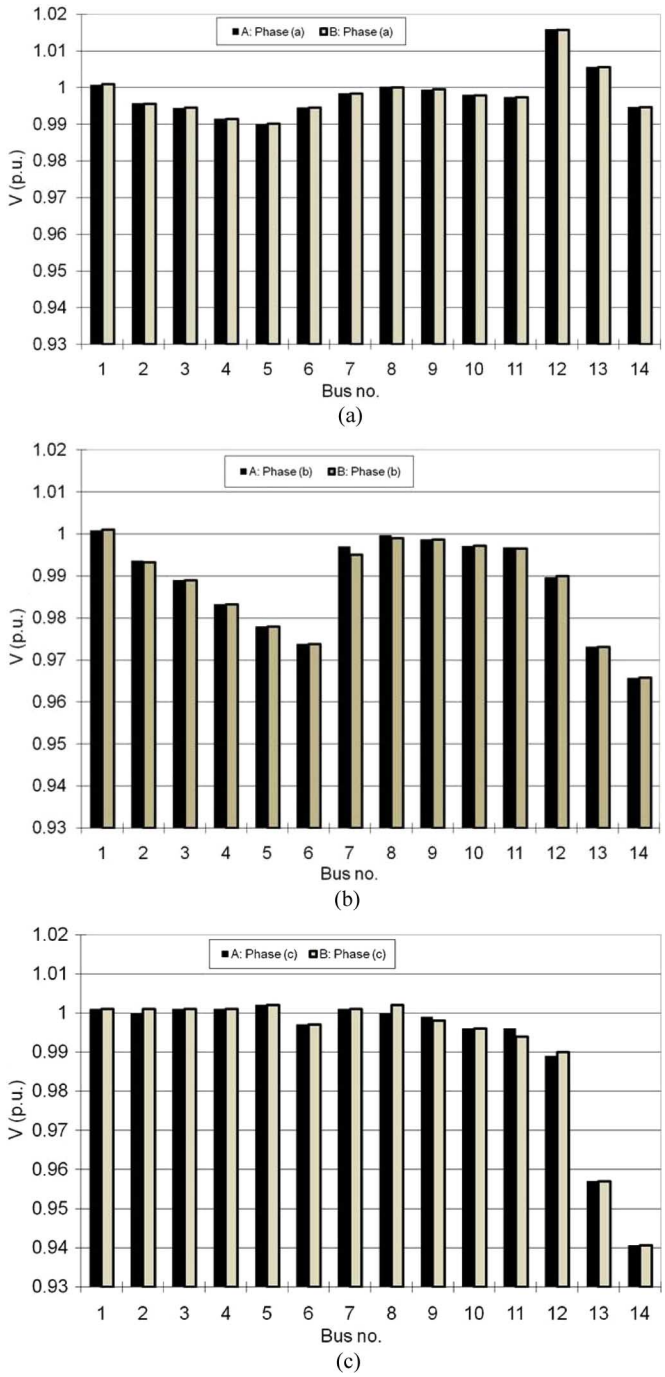

Fig. 7. Voltage magnitudes of the three-phase part of System-II. (a) PSCAD/EMTDC results. (b) Developed software results.

is calculated to be 1.0 p.u. active power at unity power-factor, as specified. This validates the PQ model representation for both the SG and the three-wire VSC-coupled DER units.

The maximum magnitude error for the five busses, in all four case studies, is less than 0.3%. The maximum phase error does not exceed 0.5%. The good agreement between the results of the two solvers indicates that the proposed steady-state DER models and the sequence-frame power-flow approach are accurate.

B. System-II

One of the CIGRE benchmark systems is selected as System-II [35], [36]. System-II is a three-phase, four-wire, medium-voltage (12.47 kV) system, Fig. 6(a), which includes five single-phase distribution subnetworks, Fig. 6(b). The system data is given in [35]. The original system parameters are given in ohms, kV and kVA. A base system of 12.47 kV and 1 MVA is used in this work for per-unitization.

System-II is an ADS candidate if it is provided by a central control center that uses bidirectional communications with the system components. The main objective of the case study performed on System-II is to demonstrate the feasibility of the developed power-flow algorithm of Fig. 4 for a relatively large and realistic size system, including DER units and single-phase laterals. All the three-phase lines are fully-transposed. The system includes a total unbalanced three-phase load of 6.46

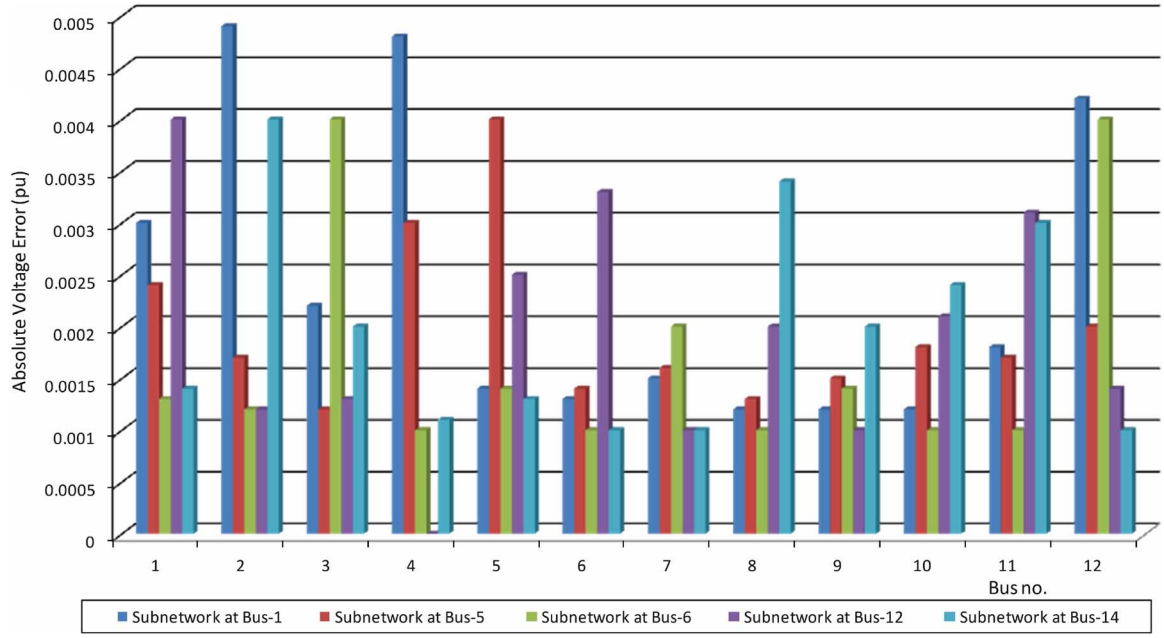

Fig. 8. Absolute error between the voltage magnitudes obtained by using the two solvers for each of the five single-phase subnetworks of System-II.

MW/3.12 MVAR. The total load of each single-phase subnetworks is 248.75 kW/90.12 kVAR.

Switches S1 and S2 in Fig. 6 are closed to form two loops, while S3 is kept open to demonstrate the capability of the developed program to handle both radial and weakly meshed ADS configurations. The system of Fig. 6 is equipped with three DER units:

- G1 is a three-wire VSC-coupled DER unit connected to Bus-8 via a three-phase transformer (100 kVA, 12.47/4.16 kV, $Y_g/\triangle$). The unit is rated at 100 kVA, 4.16 kV, and operates as a PV unit to regulate its terminal voltage at 1.0 p.u. and injects 100 kW power into the network.
- G2 is a three-phase SG unit connected to Bus-3 via a three-phase transformer (100 kVA, 12.47/4.16 kV, $Y_g/\triangle$). The unit is rated at 100 kVA, 4.16 kV, and operates as a PQ unit to inject 100 kVA power at unity power-factor.
- G3 is a three-wire VSC-coupled DER unit connected to Bus-12 via a three-phase transformer (100 kVA, 12.47/4.16 kV, $Y_g/\triangle$). The unit is rated at 100 kVA, 4.16 kV, and operates as a PQ unit to inject 100 kVA power at unity power-factor.

To verify the accuracy of the study results obtained from the developed power-flow program, the power-flow of System-II is also determined using the PSCAD/EMTDC time-domain simulation platform. The detailed models of G1, G2, and G3, as described for System-I, were also developed in the PSCAD/EMTDC-based model of System-II. The study results are shown in Figs. 7 and 8.

Fig. 7 shows the voltage magnitudes of various buses of System-II [Fig. 6(a)] deduced from the developed three-phase power-flow program and the PSCAD/EMTDC package. Fig. 8 shows the absolute error between the corresponding results obtained by the two methods for each single-phase subnetwork of Fig. 6(b).

Fig. 7 shows that the maximum error in the voltage magnitude is less than 8×10^{-3} p.u. Almost the same degree of accuracy is obtained for the power-flow results of the single-phase subnetworks. Fig. 8 indicates that the maximum error in the voltage magnitude for the single-phase subnetworks is about 5×10^{-3} p.u., and occurs at the subnetwork connected to Bus-1 of Fig. 6. The close match between the results of the PSCAD/EMTDC program and the developed program shows the accuracy of the developed power-flow algorithm and the validity of the developed DER models.

As stated in Section III, the algorithm of Fig. 4 is expected to converge faster than the coupled approach of [27]. This is shown by implementing both algorithms in the MATLAB environment to generate the complete power-flow solution of the study system of Fig. 6. The power-flow results generated by both algorithms favorably agree, and due to space limitations are not reported. However, the computational time of the software, based on the algorithm of Fig. 4, is about 72% less than that of the coupled approach. This is due to the fact that the coupled approach executes the backward/forward sweep subroutine five times more than the algorithm of Fig. 4.

V. Conclusion

This paper presents the development of a three-phase power-flow analysis method for microgirds and active distribution systems applications, under balanced and unbalanced conditions. The power-flow algorithm is developed in the sequence-component frame. This paper also develops sequence-component models of directly-coupled synchronous machine-based and electronically-coupled DER units, and incorporates them in the power-flow algorithm. The power-flow algorithm is capable of accommodating:

- different control characteristics of DER units under balanced/unbalanced utility conditions, for example, constant power (PQ)/voltage-regulated (PV) operating modes, negative sequence current mitigation, . . . etc.;
- single-phase laterals;
- single-phase and balanced/unbalanced loads;

- untransposed distribution lines;
- three-phase three- and four-wire distribution lines.

The accuracy of the power-flow algorithm and the validity of the developed models are verified by comparing power flows of two test systems with those obtained from time-domain simulation results, in the PSCAD/EMTDC package. Close agreement between the corresponding results, under balanced and unbalanced system conditions, is observed for all case studies.

REFERENCES

[1] B. Kroposki, T. Basso, and R. DeBlasio, "Microgrid standards and technologies," in *Proc. IEEE Power Energy Soc. General Meeting—Conversion and Delivery of Electrical Energy in the 21st Century*, Jul. 2008, pp. 1–4.

[2] M. Davis, "Distributed resource electric power systems offer significant advantages over central station generation and T&D power systems. I," in *Proc. IEEE Power Eng. Soc. Summer Meeting*, Jul. 2002, vol. 1, pp. 54–61.

[3] R. Lasseter, "Microgrids and distributed generation," *J. Energy Eng.*, vol. 133, no. 3, pp. 144–149, Sep. 2007.

[4] F. Kateraei, M. Iravani, and P. Lehn, "Micro-grid autonomous operation during and subsequent to islanding process," *IEEE Trans. Power Del.*, vol. 20, no. 1, pp. 248–257, Jan. 2005.

[5] F. Kateraei and M. Iravani, "Transients of a micro-grid system with multiple distributed energy resources," in *Proc. Int. Conf. Power Systems Transients*, Jun. 2005, pp. 1–6.

[6] S. Salman and S. Tan, "Investigation into protection of active distribution network with high penetration of embedded generation using radial and ring operation mode," in *Proc. 41st Int. Universities Power Eng. Conf.*, 2006, vol. 3, pp. 841–845.

[7] T. Pfajfar, I. Papic, B. Bletterie, and H. Brunner, "Improving power quality with coordinated voltage control in networks with dispersed generation," in *Proc. 9th Int. Conf. Electrical Power Quality and Utilisation*, Oct. 2007, pp. 1–6.

[8] F. Pilo, G. Pisano, and G. Soma, "Digital model of a distribution management system for the optimal operation of active distribution systems," in *Proc. Inst. Eng. Technol.C IRED SmartGrids for Distribution*, Jun. 2008, pp. 1–5.

[9] W. Xu, H. Dommel, and J. Marti, "A generalised three-phase power flow method for the initialisation of EMTP simulations," in *Proc. Int. Conf. Power System Technology*, Aug. 1998, vol. 2, pp. 875–879.

[10] T. Chen, M. Chen, K. Hwang, P. Kotas, and E. Chebli, "Distribution system power flow analysis: A rigid approach," *IEEE Trans. Power Del.*, vol. 6, no. 3, pp. 1146–1152, Jul 1991.

[11] A. Yazdani and R. Iravani, "A unified dynamic model and control for the voltage-sourced converter under unbalanced grid conditions," *IEEE Trans. Power Del.*, vol. 21, no. 3, pp. 1620–1629, Jul. 2006.

[12] C. Schauder and H. Mehta, "Vector analysis and control of advanced static VAr compensators," *Proc. Inst. Elect. Eng., Gen. Transm. Distrib.*, vol. 140, no. 4, pp. 299–306, Jul. 1993.

[13] K. Divya and P. Rao, "Models for wind turbine generating systems and their application in load flow studies," *Int. J. Elect. Power Syst. Res.*, vol. 76, no. 6, pp. 844–856, Jun. 2006.

[14] E. Haesen, J. Driesen, and R. Belmans, "Stochastic, computational and convergence aspects of distribution power flow algorithms," in *Proc. IEEE Conf. Power Technology*, Lausanne, Switzerland, Jul. 2007, pp. 1447–1452.

[15] H. Nikkhajoei and R. Iravani, "Steady-state model and power flow analysis of electronically-coupled distributed resource units," *IEEE Trans. Power Del.*, vol. 22, no. 1, pp. 721–728, Jan. 2007.

[16] H. Chen, J. Chen, D. Shi, and X. Duan, "Power flow study and voltage stability analysis for distribution systems with distributed generation," presented at the IEEE Power Eng. Soc. General Meeting, Montreal, QC, Canada, 2006.

[17] W. Bo, W. Sheng, L. Hua, and X. Hua, "Steady-state model and power flow analysis of grid connected photovoltaic power system," in *Proc. IEEE Int. Conf. Industrial Technology*, 2008, pp. 1–6.

[18] W. Kersting, *Distribution System Modeling and Analysis*, 2nd ed. New York: Taylor & Francis, 2007.

[19] D. Shirmohammadi, H. Hong, A. Semlyen, and G. Luo, "A compensation-based power flow method for weakly meshed distribution and transmission networks," *IEEE Trans. Power Syst.*, vol. 3, no. 2, pp. 753–762, May 1988.

[20] C. Cheng and D. Shirmohammadi, "A three-phase power flow method for real-time distribution system analysis," *IEEE Trans. Power Syst.*, vol. 10, no. 2, pp. 671–679, May 1995.

[21] Y. Zhu and K. Tomsovic, "Adaptive power flow method for distribution systems with dispersed generation," *IEEE Trans. Power Del.*, vol. 17, no. 3, pp. 822–827, Jul. 2002.

[22] J. Teng, "A modified Gauss-Seidel algorithm of three-phase power flow analysis in distribution networks," *Int. J. Elect. Power Energy Syst.*, vol. 24, no. 2, pp. 97–102, Feb. 2001.

[23] J. Vieira, W. Freitas, and A. Morelato, "Phase-decoupled method for three-phase power-flow analysis of unbalanced distribution systems," *Proc. Inst. Elect. Eng., Gen., Transm. Distrib.*, vol. 151, no. 5, pp. 568–574, Sep. 2004.

[24] V. Costa, M. Oliveira, and M. Guedes, "Developments in the analysis of unbalanced three-phase power flow solutions," *Int. J. Elect. Power Energy Syst.*, vol. 29, no. 2, pp. 175–182, Feb. 2007.

[25] K. Lo and C. Zhang, "Decomposed three-phase power flow solution using the sequence component frame," *Proc. Inst. Elect. Eng., Gen., Transm. Distrib.*, vol. 140, no. 3, pp. 181–188, May 1993.

[26] M. Abdel-Akher, K. Nor, and A. Rashid, "Improved three-phase power-flow methods using sequence components," *IEEE Trans. Power Syst.*, vol. 20, no. 3, pp. 1389–1397, Aug. 2005.

[27] M. Abdel-Akher, K. Nor, and A. Abdul-Rashid, "Development of unbalanced three-phase distribution power flow analysis using sequence and phase components," in *Proc. 12th Int. Middle-East Power System Conf.*, March 2008, pp. 406–411.

[28] M. Davis, "Distribution transformer load characteristic functions for residential central air conditioning," *IEEE Trans. Power App. Syst.*, vol. PAS-93, no. 1, pp. 91–99, Jan. 1974.

[29] IEEE Standards Committee, *IEEE Standard Dictionary of Electrical and Electronics Terms*. New York: Wiley, 1972.

[30] *IEEE Recommended Practice for Industrial and Commercial Power Systems Analysis*, IEEE Std. 399-1997, 1998.

[31] J. Tamura, I. Takeda, M. Kimura, M. Ueno, and S. Yonaga, "A synchronous machine model for unbalanced analyses," *Elect. Eng. Jpn.*, vol. 119, no. 2, pp. 46–59, Apr. 1997.

[32] B. Adkins, *The General Theory of Electrical Machines*. London, U.K.: Chapman and Hall, 1959.

[33] H. Karshenas and H. Saghafi, "Performance investigation of LCL filters in grid connected converters," in *Proc. IEEE/Power Eng. Soc. Transmission Distribution Conf. Expo.: Latin America*, Aug. 2006, pp. 1–6.

[34] M. Liserre, F. Blaabjerg, and S. Hansen, "Design and control of an LCL-filter-based three-phase active rectifier," *IEEE Trans. Ind. Appl.*, vol. 41, no. 5, pp. 1281–1291, Sep./Oct. 2005.

[35] 2009 CIGRE/IEEE Power Eng. Soc. Joint Symp., "Integration of wide-scale renewable resources into the power delivery system," Calgary, AB, Canada, Jul. 2009.

[36] K. Rudion, A. Orths, Z. Styczynski, and K. Strunz, "Design of benchmark of medium voltage distribution network for investigation of DG integration," in *Proc. IEEE/Power Eng. Soc. General Meeting*, 2006, pp. 1–6.

Mohamed Zakaria Kamh (GSM'08) received the B.Sc. (Hons.) and M.Sc. degrees in electrical engineering from Ain Shams University, Cairo, Egypt, in 2003 and 2007, respectively, and is currently pursuing the Ph.D. degree at the University of Toronto, Toronto, ON, Canada.

Since 2008, he has been with the Electrical and Computer Engineering Department, University of Toronto. He was an Electrical Consulting Engineer from 2003 to 2007. His research interests include power electronics and their applications in smart grids and virtual power plants.

Reza Iravani (F'03) received the B.Sc. degree in electrical engineering from Tehran Polytechnic University, Tehran, Iran, in 1976, and the M.Sc. and Ph.D. degrees in electrical engineering from the University of Manitoba, Winnipeg, MB, Canada, in 1981 and 1985, respectively.

Currently, he is a Professor with the University of Toronto, Toronto, ON, Canada. His research interests include power electronics and applications of power electronics in power systems.